JOURNAL OF Materials CHEMISTRY

Stabilisation and characterisation of a new β_{III}-phase in Zr-doped Bi_2O_3†

Isaac Abrahams,*[a] Alexandra J. Bush,[a]‡ Simon C. M. Chan,[a] Franciszek Krok[b] and Wojciech Wrobel[b]

[a]*Structural Chemistry Group, Department of Chemistry, Queen Mary and Westfield College, University of London, Mile End Road, London, UK E1 4NS. E-mail: I.Abrahams@qmw.ac.uk*

[b]*Faculty of Physics, Warsaw University of Technology, ul. Koszykowa 75, 00-662 Warsaw, Poland*

Received 4th September 2000, Accepted 28th March 2001
First published as an Advance Article on the web 24th April 2001

The solid state system Bi_2O_3:ZrO_2 has been investigated up to 28 mol% ZrO_2 using X-ray and neutron powder diffraction, ac impedance spectroscopy and differential thermal analysis. X-Ray powder diffraction has shown that a solid solution is formed with general composition $Bi_{2-x}Zr_xO_{3+x/2}$ ($0.05 \leqslant x \leqslant 0.17$) for samples calcined at 850 °C. Members of the solid solution adopt a new β-Bi_2O_3 type structure termed β_{III}, which is closely related to Pb_2F_2O. The defect structure of a sample of composition $x = 0.15$ has been determined by combined high-resolution neutron and X-ray powder diffraction. High temperature powder X-ray diffraction has been used to confirm the structure of the high temperature polymorph, which is a cubic δ-Bi_2O_3 analogue. In the β_{III}-phase, solid solution formation proceeds through an anion interstitial mechanism with respect to the hypothetical end member β_{III}-Bi_2O_3, with interstitial oxide ions located in channels parallel to the *c*-axis. The defect structure involves a pair of Zr atoms coordinated to interstitial ions in the channels. A possible conduction mechanism is proposed. Differential thermal analysis and ac impedance measurements indicate a complex phase transition to a highly conducting polymorph ($\sigma_{700} = 1.02$ S cm^{-1}) at temperatures above *ca.* 690 °C on heating. Crystal parameters: $T = 298$ K, $Bi_{1.85}Zr_{0.15}O_{3.075}$, $M = 449.49$, tetragonal, $P4_2/nmc$, $a = 7.7206(8)$, $c = 5.6370(6)$ Å, $Z = 4$, $U = 336.0(1)$ Å^3, $D_c = 8.889(3)$ g cm^{-3}; $T = 1023$ K, cubic, $Fm\bar{3}m$, $a = 5.6277(4)$ Å, $U = 178.24(4)$ Å^3, $Z = 2$, $D_c = 8.379(2)$ g cm^{-3}.

Introduction

There has been considerable interest in Bi_2O_3 and its compounds in recent years due to the high oxide ion conductivity observed in these systems.[1–3] Bi_2O_3 itself exhibits a number of polymorphs, with the highly conducting, fluorite related, δ-phase attracting particular attention. In pure Bi_2O_3 the δ-phase is only stable over a narrow temperature range 730–825 °C,[1] and much work has been carried out on stabilisation of this phase to room temperature through solid solution formation with other oxides.

Although investigations of the ternary system Bi_2O_3–CaO–ZrO_2 have been carried out,[4] as well as studies on the zirconia-rich end of the Bi_2O_3–ZrO_2 binary system,[5] little work has been published on the Bi_2O_3-rich end of this binary system. In 1964 Levin *et al.*[6] reported the phase diagram for this system which indicated a narrow solid solution range for a high temperature cubic phase, with phase separation at ambient temperatures. In the same year a study by Hund[7] suggested an extensive solid solution range of 0–70 mol% ZrO_2 that possessed the fluorite superstructure of β-Bi_2O_3. It was reported that at 60 mol% ZrO_2, the structure consists of an ideally filled anion lattice with interstitial cations, whereas pure β-Bi_2O_3 has an ideally occupied cation sublattice with vacancies in the anion sublattice.

More recently an investigation by Sorokina and Sleight[8] on the Bi_2O_3–ZrO_2 and Bi_2O_3–HfO_2 binary systems indicates that, while in the Hf system a structural analogue of $Bi_2Sn_2O_7$ is formed, no such compound is formed on Zr doping. However, they do report the existence of a defect fluorite solid solution, in the range 40–66 mol% ZrO_2, with samples calcined at 600 °C. The reported solid solution range decreases with increasing temperature of calcination until at temperatures above 750 °C only the equilibrium phases ZrO_2 and $Bi_{1.84}Zr_{0.16}O_{3.08}$ are stabilised. This latter phase they report as possessing a β-Bi_2O_3 structure.

Here we present a detailed investigation of the bismuth-rich end of the Bi_2O_3–ZrO_2 phase diagram (*ca.* 0–28 mol% ZrO_2) after high temperature calcination (850 °C) and report on the characterisation of Zr-stabilised Bi_2O_3 which, at room temperature, possesses a new β_{III}-structure, related to Pb_2F_2O.

Experimental

Preparation

Polycrystalline samples of the general composition $Bi_{2-x}Zr_xO_{3+x/2}$ ($0.03 \leqslant x \leqslant 0.33$) were prepared from appropriate amounts of Bi_2O_3 (Avocado, 99%) and ZrO_2 (Aldrich, 99%) by conventional solid state techniques. Starting materials were ground as a slurry in ethanol, using an agate mortar and pestle and dried by evaporation in air. The reaction mixture was placed in a gold boat and heated in air at 850 °C for 12 h, before quenching to room temperature. The completion of reaction

†Electronic supplementary information (ESI) available: crystal data, data collection and structural refinement data, atomic coordinates, isotropic thermal parameters, bond lengths, bond angles and contact distances for β_{III}-$Bi_{1.85}Zr_{0.15}O_{3.075}$ at 298 K and for δ-$Bi_{1.85}Zr_{0.15}O_{3.075}$ at 1023 K. See http://www.rsc.org/suppdata/jm/b0/b007136f/

‡Present address: Johnson Matthey, Catalytic Systems Division, Orchard Road, Royston, Herts, UK SG8 5HE.

was monitored by X-ray powder diffraction. Prolonged heating at high temperatures was avoided in order to minimise volatilization of Bi_2O_3. The resulting powders were orange in colour for all compositions investigated.

X-Ray diffraction

X-Ray powder diffraction data were collected on all samples using an automated Philips PW1050/30 X-ray powder diffractometer with Ni-filtered Cu-Kα radiation (λ = 1.5418 Å), in the range 5–110° 2θ, in steps of 0.02° and a scan time of 10 s per step. Data were corrected for flat plate absorption prior to refinement. No significant preferred orientation was observed in the diffraction patterns.

A high resolution X-ray powder diffraction pattern was collected on a sample with nominal composition $Bi_{1.85}Zr_{0.15}O_{3.075}$ using an INEL CPS-120 fixed position sensitive detector system on an Enraf-Nonius FR590 X-ray generator. The curved position sensitive detector allows simultaneous data collection in 4096 bins over 0–120° in 2θ. Samples were mounted on a Si-711 cut crystal and data collected in the 2θ range 0–110°, using Ge 111 monochromated Cu-Kα_1 radiation (λ = 1.54056 Å), in fixed flat-plate geometry with the incoming beam striking the sample holder at an angle of between 2 and 5°. Data were collected for a total scan time of 80 min. The measured peak positions were indexed automatically using the program TREOR[9] on a tetragonal cell of dimensions $a = 7.711$ and $c = 5.621$ Å. Systematic absences in the data were consistent with a space group assignment of $P4_2/nmc$ (no. 137).[10] High temperature (750 °C) X-ray powder diffraction data were also collected on this sample using a Siemens D5000 X-ray powder diffractometer with secondary beam graphite monochromated Cu-Kα radiation (λ = 1.5418 Å). Data were collected in flat plate $\theta/2\theta$ mode using a linear position sensitive detector in the 2θ range 10–80°, in steps of 0.01431°, with a scan time of 2 s per step.

Neutron diffraction

High-resolution powder neutron diffraction data were collected on the HRPD diffractometer at the ISIS facility, Rutherford Appleton Laboratory. Approximately 10 cm^3 of powdered sample corresponding to the nominal composition $Bi_{1.85}Zr_{0.15}O_{3.075}$ was placed in a 12 mm diameter cylindrical vanadium can. Data were collected at room temperature from a sample mounted 1 m in front of back-scattering detectors, in the time of flight range 30–130 ms.

Crystallographic refinements

The unit cell obtained from indexing of the high resolution X-ray data was similar to that of the β-phase of Bi_2O_3. However, unlike $Bi_{1.85}Zr_{0.15}O_{3.075}$, β-$Bi_2O_3$ crystallises in the tetragonal space group $P42_1c$ (no. 114).[10] A search of the ICSD database[11] revealed that Pb_2F_2O [12] has similar unit cell dimensions to $Bi_{1.85}Zr_{0.15}O_{3.075}$ and the same space group, $P4_2/nmc$. The structural parameters of this compound were used in a starting model for structure refinement with appropriate substitution of Bi or Zr for Pb and O for F. Structure refinement was carried out using the Rietveld method with all calculations on the combined X-ray and neutron data performed using GSAS.[13] A small amount of ZrO_2 was also refined as a secondary phase. A polynomial background was refined after appropriate background subtraction for the vanadium can in the neutron data. Scattering factors for neutral atoms were assumed for the X-ray refinement and the data were corrected for flat plate absorption. Two models for the solid solution mechanism were tested on the neutron data, *viz.*: (i) an anion interstitial model and (ii) a cation vacancy model both with respect to the hypothetical solid solution end member β_{III}-Bi_2O_3. In the final refinements isotropic thermal parameters were refined for all atoms in the primary phase with those of Bi and Zr tied together. It is interesting to note that an X-ray diffraction pattern of a compound with composition $Bi_{7.38}Zr_{0.62}O_{12.31}$ is recorded in the PDF-2 database as possessing space group $P\bar{4}2_1c$.[14] The recorded X-ray pattern is virtually identical to those seen in the present study but significantly different to that of β-Bi_2O_3.[15] Since the systematic absences in $P\bar{4}2_1c$ are a subset of those in $P4_2/nmc$ it is possible to successfully index the diffraction pattern in the lower symmetry space group. However, the full structure refinement in the present study indicate that the correct space group assignment for this phase is actually $P4_2/nmc$.

Unit cell parameters for $Bi_{2-x}Zr_xO_{3+x/2}$ solid solutions were refined by whole profile fitting of their X-ray powder diffraction patterns using the Rietveld method, on samples prepared from Bi_2O_3:ZrO_2 mixtures in the approximate composition range 3–28 mol% ZrO_2. Data were refined in the 2θ range 25–110° using the program GSAS.[13] The anion interstitial model obtained from the neutron diffraction refinements was used as a starting model. A pseudo-Voigt peak shape was refined along with scale, polynomial background coefficients and zero-point correction. Scattering factors for neutral atoms were assumed. The only structural parameters refined were the Bi/Zr isotropic thermal parameters and the lattice parameters.

The high temperature structure refinement was carried out using the Rietveld method with calculations performed using GSAS.[13] A starting model for refinement was based on the δ-Bi_2O_3 structure.[16] A polynomial background was refined and scattering factors for neutral atoms were assumed. Crystal and refinement parameters for both δ and β_{III} phases are summarised in Table 1.

CCDC reference numbers 162509 and 162510. See http://www.rsc.org/suppdata/jm/b0/b007136f/ for crystallographic data in CIF or other electronic format.

Differential thermal analysis

DTA was performed on all samples using a Setaram Labsys combined TG/DTA, with a heating and cooling rate of 20 °C min^{-1}, from room temperature to 850 °C under an N_2 atmosphere. Reaction temperatures were established by heating unreacted powders on a Perkin Elmer 7 Series Thermal Analysis System at a rate of 10 °C min^{-1}.

ac Impedance measurements

The electrical conductivity measurements were performed by means of ac impedance spectroscopy, using a Solartron 1255/1286 system, in the frequency range 1 Hz to 5×10^5 Hz, over the approximate temperature range 250–770 °C. For each sample, ac impedance measurements were performed over two cycles of heating and cooling. Measurements were made under isothermal conditions after temperature stabilisation had been achieved at selected temperatures. The duration of each heating/cooling cycle was approximately 48 h. Spectra were collected for $Bi_{2-x}Zr_xO_{3+x/2}$ samples of nominal compositions $x = 0.07$, 0.11, 0.15 and 0.21. Samples for impedance measurements were prepared as sintered pellets. Pellets were initially formed by uniaxial pressing at low pressures and then isostatically at 3500 kg cm^{-2}. Sintering was carried out in air at 820 °C for 16 h and pellets subsequently cut using a diamond saw into rectangular bars. Platinum electrodes were deposited by cathodic discharge sputtering. Pellet densities of 97–99% theoretical density were obtained.

Table 1 Crystal and refinement parameters for $Bi_{1.85}Zr_{0.15}O_{3.075}$

	β_{III}-phase (298 K)	δ-phase (1023 K)
Formula	$Bi_{1.85}Zr_{0.15}O_{3.075}$	$Bi_{1.85}Zr_{0.15}O_{3.075}$
M	449.49	449.49
Crystal system	Tetragonal	Cubic
Space group	$P4_2/nmc$	$Fm\bar{3}m$
Cell dimensions/Å	$a=7.7206(8)$, $c=5.6370(6)$	$a=5.6277(4)$
Volume/Å^3	336.0(1)	178.24(4)
Z	4	2
D_c/g cm^{-3}	8.889(3)	8.379(2)
Appearance	Orange powder	Orange powder
Radiation	Pulsed neutrons, X-Ray (Cu-Kα, $\lambda=1.5418$ Å)	X-Ray (Cu-Kα, $\lambda=1.5418$ Å)
Data ranges collected	Neutron 0.622–2.695 Å X-Ray 5–110° 2θ	20–80° 2θ
Data range refined	Neutron 0.634–2.488 Å X-Ray 20–110° 2θ	20–80° 2θ
No. of data points	Neutron 4405 X-Ray 4499	4193
No of independent reflections for primary phase	Neutron 362 X-Ray 130	8
R-factors	Neutron $R_p=0.0701$, $R_{wp}=0.0754$, $R_{ex}=0.0216$, $R_{F^2}=0.1906$ X-ray $R_p=0.1029$, $R_{wp}=0.1310$, $R_{ex}=0.1361$, $R_{F^2}=0.1416$	$R_p=0.0413$, $R_{wp}=0.0533$, $R_{ex}=0.0427$, $R_{F^2}{}^2=0.2163$

Results and discussion

Evidence for solid solution formation

The X-ray powder diffraction patterns for samples with starting compositions less than $x=0.05$ showed a mixture of a dominant tetragonal phase and a secondary phase corresponding to α-Bi_2O_3. In the composition range $0.05\leqslant x\leqslant 0.19$, α-$Bi_2O_3$ peaks were undetectable and the tetragonal phase only was observed. Above $x=0.19$, a weak secondary phase corresponding to ZrO_2 was observed. The tetragonal primary phase seen was successfully indexed in the space group $P4_2/nmc$ with unit cell dimensions $a\approx 7.72$ and $c\approx 5.63$ Å. Fig. 1 shows the variation in refined unit cell parameters with sample composition. The data show a decrease in all cell parameters on initial substitution reaching a minimum at $x=0.09$. There then follows a classical Vegard type linear increase in all parameters to a maximum at $x=0.17$, with a subsequent small drop in the *a*-axis dimension which is also reflected in the volume. Above $x=0.19$ there is a levelling off of cell parameters, while at higher compositions (above $x=0.25$) some fluctuation in cell parameters is observed. These results suggest that the solid solution limit lies at around $x=0.17$ which is close in composition to the equilibrium phase described by Sorokina and Sleight,[8] $Bi_{1.84}Zr_{0.16}O_{3.08}$. At higher compositions trace amounts of ZrO_2 are observed in the X-ray pattern. This may account for the fluctuation in cell parameters at high compositions, as the second phase in these X-ray patterns was not refined and may have led to greater uncertainty in the refined cell parameters. It should be noted that compositions quoted are nominal as it is likely that small amounts of Bi_2O_3 (*ca.* 1 wt% by measured weight loss) are lost through volatilisation during reaction. Although not detected in the X-ray diffraction patterns, due to the dominant scattering of the Bi containing component, some ZrO_2 was observed in the neutron diffraction pattern of the $x=0.15$ sample. The results are consistent with a solid solution of general formula, $Bi_{2-x}Zr_xO_{3+x/2}$ ($0.05\leqslant x\leqslant 0.17$).

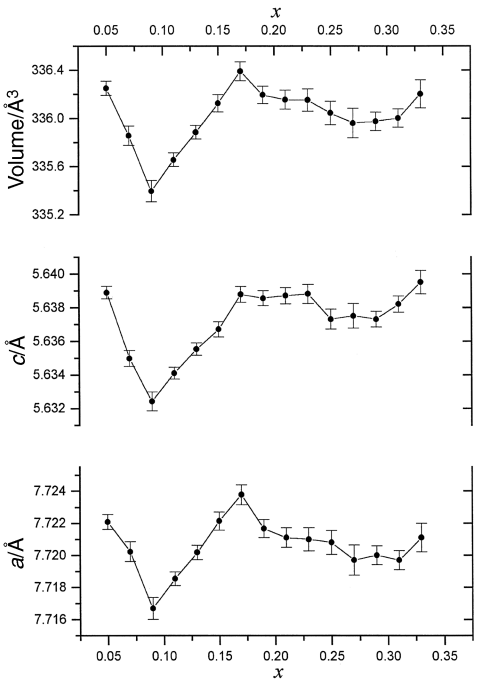

Fig. 1 Variation of unit cell parameters with composition in β_{III}-$Bi_{2-x}Zr_xO_{3+x/2}$.

The observed variation in cell dimensions on solid solution formation might be explained by two parallel mechanisms, *viz.*: (i) substitution of trivalent Bi ($r=1.02$ Å)[17] by the smaller tetravalent Zr ($r=0.72$ Å)[17] and (ii) incorporation of additional O^{2-} ions into the vacant channel sites with an accompanying expansion of the channel radius. The results would suggest that, initially, the unit cell parameter variation is dominated by the first effect with a consequent decrease in all parameters, and that between *ca.* $x=0.09$ to $x=0.17$ the second effect is dominant. Nevertheless, because of the sharpness of the transition at $x=0.09$, we cannot exclude the influence of other factors.

Crystal structure of β_{III}-$Bi_{1.85}Zr_{0.15}O_{3.075}$

The crystal structure of a representative member of the solid solution series ($x=0.15$) was refined using high resolution neutron diffraction at 298 K. The structure of β_{III}-$Bi_{1.85}Zr_{0.15}O_{3.075}$ is best described by first considering an idealised model. The idealised structure, which is similar to that of Pb_2F_2O,[12] is made up of two-dimensional corrugated layers of bismuth oxide stacked in the *c*-axis direction (Fig. 2). Bi $6s^2$ lone pairs point out of the layers where they prevent the close approach of oxygen atoms in the layers above and below. Bi is essentially coordinated to three oxygen atoms in a trigonal pyramidal geometry. The Bi and O atoms are arranged in

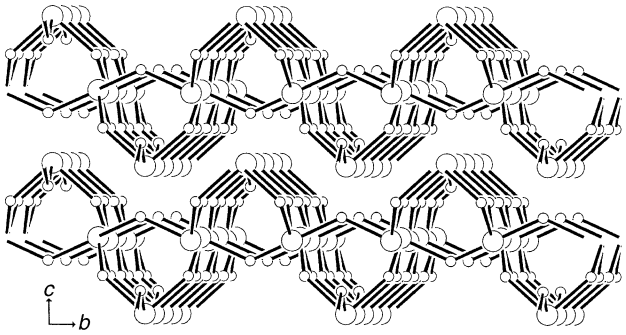

Fig. 2 Idealised layer structure in β_{III}-$Bi_{1.85}Zr_{0.15}O_{3.075}$. Large and small open circles represent Bi and O atoms, respectively.

Table 2 Neutron data refinement parameters for solid solution mechanism models in Bi_2O_3(86 mol%) : ZrO_2 (14 mol%)

Model	R_{wp}	R_p	R_{F^2}	N_{var}	N_{obs}
Anion interstitial	0.0755	0.0701	0.1964	30	4405
Cation vacancy	0.0762	0.0713	0.1915	28	4405

convoluted Bi_4O_4 rings, which are themselves linked by O atoms. Stacking of these rings between layers results in channels parallel to the *c*-axis (Fig. 3). Pairs of Bi atoms are located at positions on opposite sides of the channels and are mutually perpendicular to those in the adjacent layer. The stacking of the layers in this way results in an interstitial inter-layer anion site with tetrahedral coordination to bismuth. The Bi $6s^2$ lone pairs point approximately towards this interstitial site.

In order to determine the details of the defect structure two possible models for the solid solution mechanism were tested. The first involved an anion interstitial mechanism, with respect to the hypothetical solid solution end member β_{III}-Bi_2O_3, corresponding to a general formula, $Bi_{2-x}Zr_xO_{3+x/2}$. In this case the anion content increases with respect to x. The second possible mechanism involved cation vacancies, where the occupancy of the anion sublattice remains constant with respect to x. The general formula for this second mechanism is given by $Bi_{(12-6x)/(6+x)}Zr_{(6x/6+x)}\square_{2x/(6+x)}O_3$ where $\square$ represents cation vacancies. No evidence was seen in the difference maps generated from the neutron data for anion interstitials, however, at $x=0.15$ the number of these interstitials would be very small and probably beyond the detection limit of the technique. Density measurements proved to be inconclusive in distinguishing between these two models.

Rietveld refinement of the two models using the neutron data for the $x=0.15$ sample was carried out. Structural and thermal isotropic thermal parameters were refined for all atoms in the primary phase. Table 2 summaries the *R*-factors and related parameters for the two refinements. The ratio of the weighted profile *R*-factors for the two refinements is 1.0093. Using the Hamilton F-Test,[18] it is possible to test the hypothesis that the anion interstitial model represents a better description of the structure (degrees of freedom = 4405 − 30, dimension of hypothesis = 30 − 28 = 2). For the hypothesis to be proved the *R*-factor ratio needs to be above a significance value, which at the 0.005 confidence level can be calculated as 1.0012. Thus we can say that the anion interstitial model is a significantly better description of the defect structure.

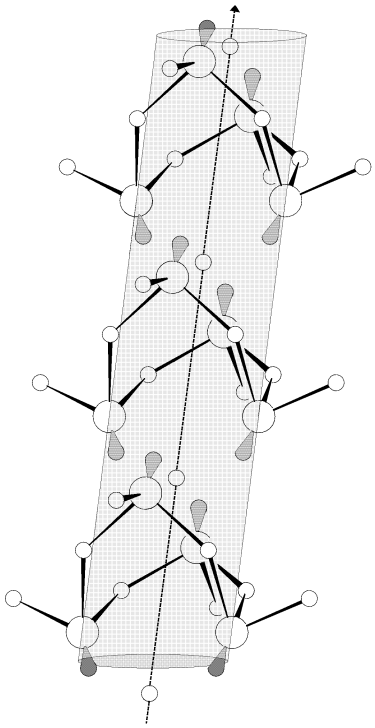

Fig. 3 Arrangement of Bi $6s^2$ lone pairs in channels (shaded) of β_{III}-$Bi_{1.85}Zr_{0.15}O_{3.075}$. Large and small open circles represent Bi and O atoms, respectively. Lone pair orbitals are shown schematically, with positions calculated at a distance of 0.98 Å along the BiO_3 pyramid axis.

The final refinements were therefore carried out on the anion interstitial model using combined X-ray and neutron data. During refinement large isotropic thermal parameters on O(2) suggested that oxygen on this site is shifted away from the ideal 8*f* site at 0.04, 0.04, 0.25 and therefore oxygen on this site was allowed to refine in a general 16*h* position with fixed half site occupancy. Table 3 shows the final refined parameters for β_{III}-$Bi_{1.85}Zr_{0.15}O_{3.075}$, with the corresponding fitted diffraction profiles in Fig. 4. Significant contact distances and angles are presented in Table 4.

Bi in the structure is located in a pyramidal site with the lone pair on Bi preventing close approach of oxygen atoms in the direction of the lone pair orbital. Zr in contrast possesses no non-bonding valence electrons and would be expected locally to adopt a more regular coordination environment. Therefore, the Zr and Bi positional parameters were allowed to refine independently, however, their isotropic thermal parameters were tied to each other.

Defect structure and conduction mechanism in β_{III}-$Bi_{1.85}Zr_{0.15}O_{3.075}$

To satisfy the coordination requirements of Zr, it is likely that two Zr atoms would have to be directly opposite each other on

Table 3 Final refined atomic parameters for β_{III}-$Bi_{1.85}Zr_{0.15}O_{3.075}$ at 25 °C

Atom	Site	*x*	*y*	*z*	Occupancy	U_{iso}/Å^2
Bi	8*g*	0.25	0.0025(2)	0.0097(2)	0.925[a]	0.0214(3)
Zr	8*g*	0.25	0.026(2)	0.040(3)	0.075[a]	0.0214(3)
O(1)	4*d*	0.25	0.25	−0.1469(2)	1.00[a]	0.0220(4)
O(2)	16*h*	0.4611(2)	−0.0630(2)	−0.2227(3)	0.5[a]	0.0258(4)
O(3)	4*c*	0.25	−0.25	0.206(6)	0.075[a]	0.059(10)

[a]Fixed parameters.

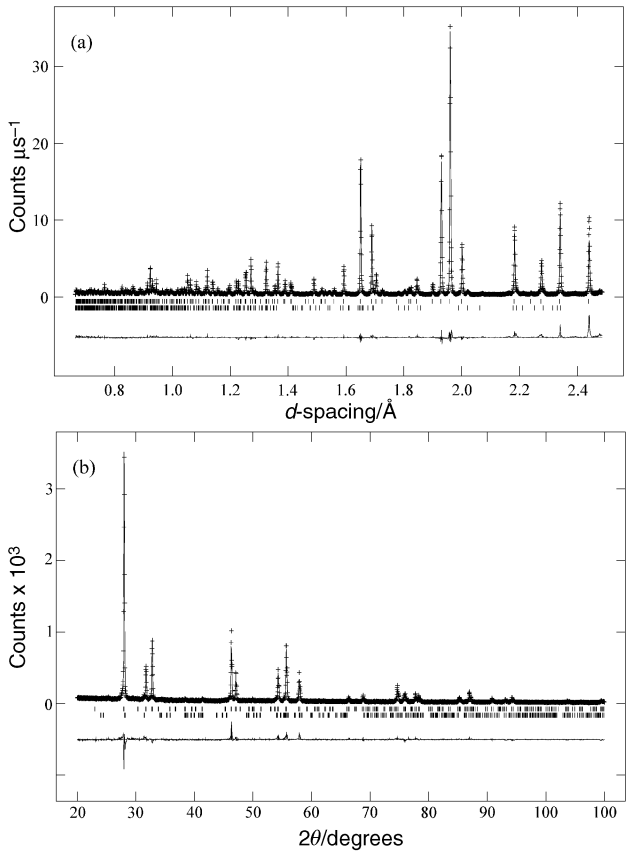

Fig. 4 Fitted diffraction profiles for β_{III}-$Bi_{1.85}Zr_{0.15}O_{3.075}$ at 298 K showing, observed (points), calculated (line) and difference (lower) profiles; (a) neutron data, (b) X-ray data. Markers indicate reflection positions.

the sides of a channel sharing a coordinated interstitial oxygen, O(3), within the channel. Fig. 5 shows the location of zirconium and interstitial oxygen sites with respect to the channels.

In order to visualise possible routes for conduction it is helpful to examine the anion sites in more detail. The bismuth atoms are arranged in a cubic close packed array with all octahedral sites vacant. O(1) and O(2) atoms are located in $\frac{3}{4}$ of

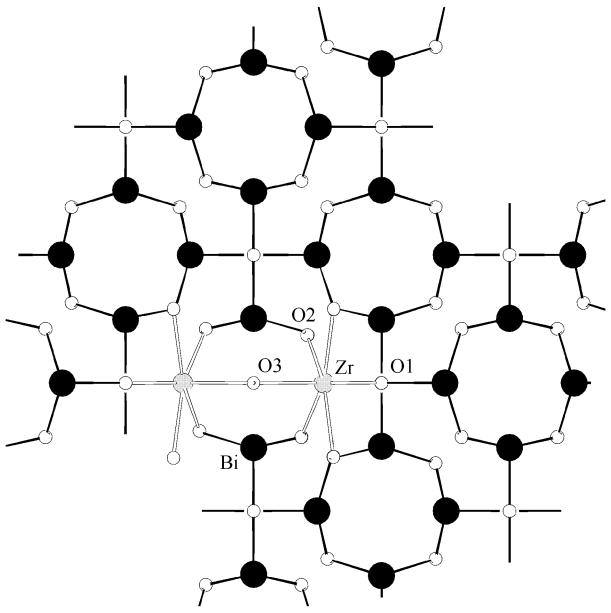

Fig. 5 Projection down *c*-axis of β_{III}-$Bi_{1.85}Zr_{0.15}O_{3.075}$ showing details of the defect structure.

Table 4 Significant distances (Å) and angles (°) in β_{III}-$Bi_{1.85}Zr_{0.15}O_{3.075}$ at 25 °C

Bi–O(1)	2.105(1)	Zr–O(1)	2.03(2)
Bi–O(2)	2.152(2) × 2	Zr–O(2)	2.31(1) × 2
Bi–O(2′)	2.192(2) × 2	Zr–O(3)	2.33(2)
		Zr–O(2′)	2.35(1) × 2
		Zr–O(1‴)	2.47(2) × 2
		Zr–O(2″)	2.472(7) × 2
		Zr–O(3′)	2.57(2)
O(1)–Bi–O(2)	87.59(6) × 2	O(1)–Zr–O(2)	85.4(5) × 2
O(1)–Bi–O(2′)	79.79(6) × 2	O(1)–Zr–O(3)	172.3(12)
O(2)–Bi–O(2)	98.5(1)	O(1)–Zr–O(2′)	77.6(5) × 2
O(2)–Bi–O(2′)	90.88(7) × 2	O(1)–Zr–O(1‴)	76.9(6)
O(2′)–Bi–O(2′)	82.41(9)	O(1)–Zr–O(2″)	96.8(5) × 2
		O(1)–Zr–O(3′)	177.5(14)
		O(2)–Zr–O(2)	89.9(5)
		O(2)–Zr–O(3)	89.2(7) × 2
		O(2)–Zr–O(2′)	83.2(5) × 2
		O(2)–Zr–O(1‴)	131.8(4) × 2
		O(2)–Zr–O(2″)	70.39(9) × 2
		O(2)–Zr–O(3′)	96.4(7) × 2
		O(3)–Zr–O(2′)	96.4(8) × 2
		O(3)–Zr–O(1‴)	110.8(10)
		O(3)–Zr–O(2″)	86.5(5) × 2
		O(3)–Zr–O(3′)	10.2(15)
		O(2′)–Zr–O(2′)	75.7(5)
		O(2′)–Zr–O(1‴)	133.8(5) × 2
		O(2′)–Zr–O(2″)	77.7(1) × 2
		O(2′)–Zr–O(3′)	104.4(7) × 2
		O(1‴)–Zr–O(2″)	67.8(3) × 2
		O(1‴)–Zr–O(3′)	100.6(8)
		O(2″)–Zr–O(2″)	128.9(6)
		O(2″)–Zr–O(3′)	82.2(5) × 2

Symmetry relations: $' = -y$, $(x+0.5)-1$, $(-z+0.5)-1$; $'' = -x-1$, $-y$, $-z$; $''' = y$, x, $z+0.5$.

the available tetrahedral sites, but are bonded to only two Bi atoms along a single edge of their respective tetrahedra. These tetrahedra are stacked in edge sharing columns running parallel to the *c*-axis with columns linked to each other by further edge sharing. The remaining tetrahedra, which contain the interstitial O(3) oxygens, are arranged in edge sharing columns and constitute the channels through the Bi_4O_4 rings.

The Bi–O(1) and Bi–O(2) bond lengths indicate that these bonds are covalent in character. Therefore, O(1) and O(2) are unlikely to be involved directly in conduction and hence the movement of oxide ions between O(3) sites represents the major contribution to oxide ion conductivity in this phase. In close packed structures, ions generally prefer conduction pathways that involve passing through the shared faces of polyhedra. In the case of β_{III}-$Bi_{1.85}Zr_{0.15}O_{3.075}$ an oxide ion located in the O(3) site would pass through a face into a vacant octahedral site. However, at this point the oxide ion would have to pass through another face into an occupied tetrahedral site (O(1) or O(2)), before completing its journey through another octahedral site into a vacant O(3) tetrahedral site. The occupied tetrahedral site represents a significant barrier to conduction along this pathway, although it may be possible for transient oxide ions to pass through these sites, remembering that the O(1) and O(2) oxygens are bonded preferentially to one side of their respective tetrahedra.

A more plausible mechanism involves conductivity of oxide ions along the channels parallel to the *c*-axis. These channels involve two tetrahedral sites, *viz.*: the O(3) site which contains the interstitial ion and a vacant tetrahedral site located at the centre of a Bi_4O_4 ring. The pathway would therefore be through shared tetrahedral edges rather than through faces. Critically, the Bi atoms along this shared edge are not bonded to each other through an oxygen and therefore a degree of flexibility is predicted. In addition, the Bi–Bi distance along this shared edge is 3.898(3) Å leaving a large opening for transient oxide ions.

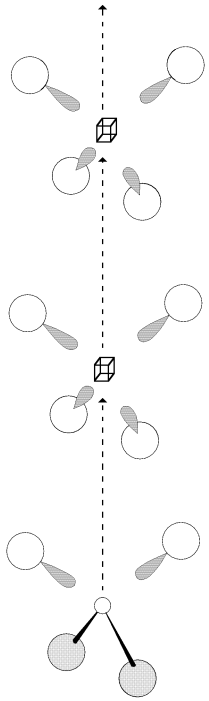

Fig. 6 Schematic representation of conduction mechanism in β_{III}-$Bi_{1.85}Zr_{0.15}O_{3.075}$, showing O(3) conduction pathway (broken arrow). Shaded, large open and small open circles represent Zr, Bi and O atoms, respectively. Cubes represent vacant O(3) sites.

In order for conduction to occur, oxide ions located in the centre of the channels have to hop between vacant tetrahedral sites, until they reach a pair of Zr atoms to which they can coordinate. However, the vast majority of the metal atoms around the channels are Bi and as described above, the Bi atoms are arranged in pairs, with their $6s^2$ lone pairs of electrons pointing approximately towards vacant O(3) sites within the channel. Therefore each vacant O(3) site has four Bi lone pairs tetrahedrally arranged around it. This type of interstitial site is in contrast to other bismuth oxide-based solid electrolytes such as the BIMEVOXes[19,20] and $Bi_2Al_4O_9$,[21] where typically the interstitial conduction site is linear in coordination with two Bi lone pairs pointing directly towards it. Fig. 6 shows a schematic representation of the proposed mechanism of oxide ion conductivity in β_{III}-$Bi_{1.85}Zr_{0.15}O_{3.075}$. As in other Bi_2O_3 based systems the mechanism relies on the polarisibility of the Bi $6s^2$ lone pair of electrons.

Electrical conductivity

The impedance spectra in the low temperature region of $Bi_{2-x}Zr_xO_{3+x/2}$ (where $x=0.07$, 0.11, 0.15 and 0.21) consisted generally of two semicircles, considered as the bulk sample and grain boundary contributions to total resistance. Separation of these contributions was not clear at higher temperatures and therefore only the total conductivities are discussed here. Although at low temperatures Bi_2O_3 itself has a significant electronic contribution to total conductivity,[2] it is assumed here that, as in pure Bi_2O_3, the high temperature conductivity is mainly ionic.

The Arrhenius plots of total conductivity for all the compositions studied were similar. A representative Arrhenius plot for $Bi_{1.89}Zr_{0.11}O_{3.055}$ ($x=0.11$) over heating and cooling cycles is shown in Fig. 7. The plot shows two linear regions. There is a large jump in total conductivity between the two linear regions, which occurs at about 700 °C in heating cycles with a corresponding decrease observed during cooling, but at a lower temperature of approximately 600 °C. Electrical parameters for the four compositions studied are summarised

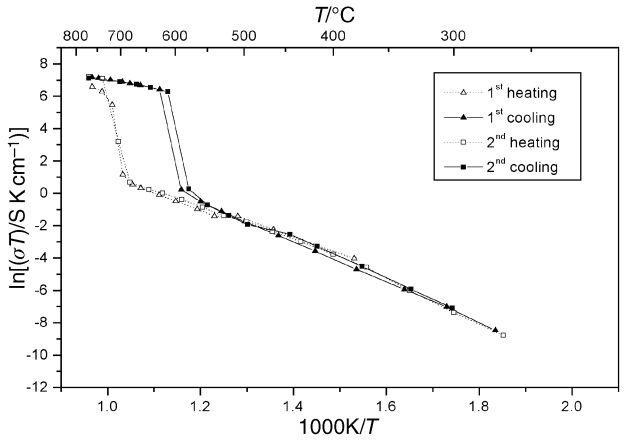

Fig. 7 Arrhenius plot of conductivity for $Bi_{1.89}Zr_{0.11}O_{3.055}$ over successive heating and cooling cycles.

Table 5 Conductivity parameters for compositions in the system $Bi_{2-x}Zr_xO_{3+x/2}$

x	σ_{300}/S cm^{-1}	ΔE_{LT}/eV	σ_{700}/S cm^{-1}	ΔE_{HT}/eV
0.07	6.49×10^{-7}	1.14	0.85	0.45
0.11	1.19×10^{-6}	1.13	1.01	0.44
0.15	3.92×10^{-7}	1.19	0.60	0.43
0.21	2.94×10^{-7}	1.04	0.40	0.42

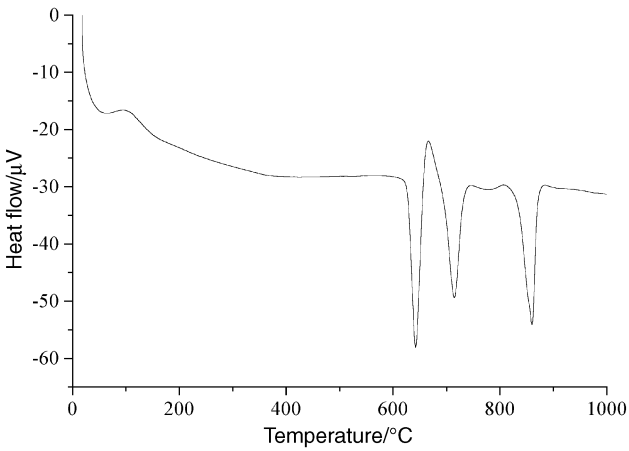

Fig. 8 Differential thermal analysis trace for $Bi_{1.85}Zr_{0.15}O_{3.075}$.

in Table 5. Data correspond to the first cooling cycle where the linear range of the high temperature is more extensive. Generally the activation energies in the highly conducting high temperature region (ΔE_{HT}) are significantly lower than those in the low temperature region (ΔE_{LT}). The total conductivities at 700 °C in the solid solution range are of the order of 1 S cm^{-1} and are comparable in magnitude to the best oxide ion conductors based on Bi_2O_3.[2]

Thermal analysis

Differential thermal analysis traces for all compositions showed similar features. A representative DTA trace for synthesised material ($x=0.15$) on heating is shown in Fig. 8. Three major thermal events are evident, *viz.*: a sharp endotherm at 642 °C immediately followed by a second endotherm at 714 °C, with a last endotherm at 860 °C corresponding to melting. At 750 °C the δ-phase is seen in high temperature X-ray patterns and therefore the endotherm seen at 714 °C must be due to a solid state transition to this phase. The first thermal event at 642 °C is therefore associated

Table 6 Final refined atomic coordinates and isotropic thermal parameters for δ-$Bi_{1.85}Zr_{0.15}O_{3.075}$ at 750 °C; and selected bond lengths (Å) and angles (°) for δ-$Bi_{1.85}Zr_{0.15}O_{3.075}$ at 750 °C

(a)

Atom	Site	x	y	z	Occupancy	U_{iso}/Å^2
Bi/Zr	4*a*	0.0	0.0	0.0	0.925/0.075[a]	0.013(1)
O	8*c*	0.25	0.25	0.25	0.76785[a]	0.04(1)

(b)

Bi/Zr–O	2.4369(1) × 8
O–Bi/Zr–O′	70.529(6) × 12
O–Bi/Zr–O″	109.471(3) × 12
Bi/Zr–O–Bi/Zr‴	109.471(3) × 6

[a]Fixed parameters. Symmetry relations: $'=x, y, -z$; $''=-x, -y, z$; $'''=x, y+0.5, z+0.5$.

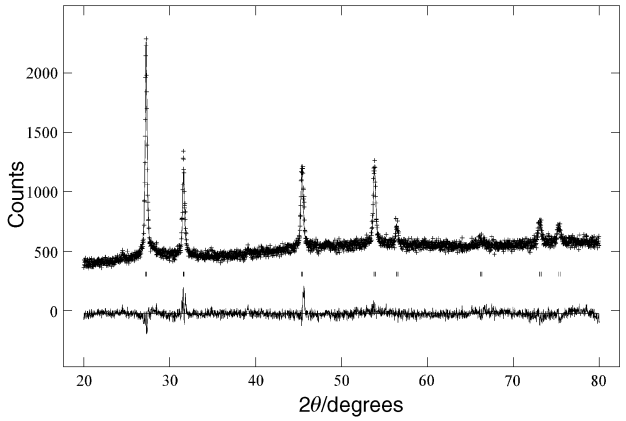

Fig. 9 Fitted diffraction profile for δ-$Bi_{1.85}Zr_{0.15}O_{3.075}$ at 1023 K showing, observed (points), calculated (line) and difference (lower) profiles. Markers indicate reflection positions.

with a preliminary phase transition, the exact nature of which is unclear. However, by comparison to pure Bi_2O_3, the temperature region 642–714 °C may be associated with stabilisation of a γ-phase intermediate.[22,23]

Structure of δ-$Bi_{1.85}Zr_{0.15}O_{3.075}$

Fig. 9 shows the fitted X-ray diffraction pattern for $Bi_{1.85}Zr_{0.15}O_{3.075}$, at 750 °C and confirms the structure is a δ-phase. The atomic coordinates, isotropic thermal parameters and significant bond lengths and angles are presented in Table 6. The bond lengths found in this study are longer than those reported in the literature[16] due to the high temperature at which this work was carried out. It was assumed that Zr substitutes for Bi in the structure. The structure of δ-$Bi_{1.85}Zr_{0.15}O_{3.075}$ was found to be identical to δ-Bi_2O_3 where full structural details can be found in the literature.[16,24–26]

Conclusions

At ambient temperature a new β_{III}-phase related to β-Bi_2O_3 phase was obtained for solid solutions of general formula $Bi_{2-x}Zr_xO_{3+x/2}$ $(0.05 \leqslant x \leqslant 0.17)$. In the structure of $Bi_{1.85}Zr_{0.15}O_{3.075}$, the Bi $6s^2$ lone pairs of electrons point into a central channel, through which oxide ion migration can occur. Substitution of Zr for Bi in the lattice results in the introduction of interstitial oxide ions into these conduction channels.

The Arrhenius plots of conductivity and the differential thermal analysis data clearly show a complex phase transition from the β_{III}-phase, which has a defect fluorite structure with ordered vacancies in the oxide sub-lattice, to δ-Bi_2O_3, which has a fluorite structure with disordered vacancies on the oxygen sub-lattice.

Acknowledgements

We would like to thank Dr. Jonathan Knowles at the Eastman Dental Institute for DTA results, Dr R. M. Wilson in the Department of Biophysics in Relation to Dentistry at QMW for high resolution X-ray data and Dr I. M. Gibson at the IRC in Biomedical Materials at QMW for high temperature X-ray data. We gratefully acknowledge the EPSRC for a project studentship for A. J. B. and for neutron beam time at the Rutherford Appleton Laboratory. We also wish to thank the CDS service at the Daresbury Laboratory for access to the ICSD database, and Dr. K. S. Knight at the Rutherford Appleton Laboratory for his help in neutron data collection. We also gratefully acknowledge financial support from the Polish State Committee for Scientific Research and the Royal Society of Chemistry for a Journals Grant for International Authors.

References

1 G. Mairesse, in *Fast Ion Transport in Solids*, ed. B. Scrosati, A. Magistris, C. M. Mari and G. Mariotto, Kluwer Academic Publ., Dordrecht, The Netherlands, 1993, p. 271.
2 P. Shuk, H.-D. Wiemhofer, U. Guth, W. Gopel and M. Greenblatt, *Solid State Ionics*, 1996, **89**, 179.
3 J. C. Boivin and G. Mairesse, *Chem. Mater.*, 1998, **10**, 2870.
4 K. Z. Fung, J. Chen and A. V. Virkar, *J. Am. Ceram. Soc.*, 1993, **76**, 2403.
5 A. Gulino, S. La Delfa, I. Fragalà and R. G. Egdell, *Chem. Mater.*, 1996, **8**, 1287.
6 E. M. Levin, C. R. Robbins and H. F. McMurdie, in *Phase Diagrams for Ceramists*, ed. M. K. Reser, American Ceramic Society, Westerville, Ohio, 1964, p. 128.
7 V. F. Hund, *Z. Anorg. Allg. Chem.*, 1964, **333**, 248.
8 L. Sorokina and A. W. Sleight, *Mater. Res. Bull.*, 1998, **33**, 1077.
9 P. E. Werner, L. Eriksson and M. Westdahl, *J. Appl. Crystallogr.*, 1985, **18**, 367.
10 *International Tables for Crystallography – Volume A Space Group Symmetry*, ed. T. Hahn, Kluwer Academic Publ., Dordrecht, The Netherlands, 3rd edn., 1992.
11 ICSD—Inorganic Crystal Structure Database, Release 9901, FIZ-Karlsruhe, Germany, 1999; D. A. Fletcher, R. F. McMeeking and D. Parkin, *J. Chem. Inf. Comput. Sci.*, 1996, **36**, 746.
12 B. Aurivillius, *Chem. Scr.*, 1976, **10**, 156.
13 A. C. Larson and R. B. von Dreele, Los Alamos National Laboratory Report No. LAUR-86-748, 1987.
14 ICDD Powder Diffraction File, PDF-2, ICDD, Pennsylvania, USA, 1998, Card 44-445.
15 ICDD Powder Diffraction File, PDF-2, ICDD, Pennsylvania, USA, 1998, Card 27-50.
16 H. A. Harwig, *Z. Anorg. Allg. Chem.*, 1978, **444**, 151.
17 R. D. Shannon and C. T. Prewitt, *Acta Crystallogr., Sect. B*, 1969, **25**, 925; R. D. Shannon and C. T. Prewitt, *Acta Crystallogr., Sect. B*, 1970, **26**, 1046.
18 W. C. Hamilton, *Acta Crystallogr.*, 1968, **18**, 502.
19 I. Abrahams, F. Krok and J. A. G. Nelstrop, *Solid State Ionics*, 1996, **90**, 57.
20 I. Abrahams, J. A. G. Nelstrop, F. Krok and W. Bogusz, *Solid State Ionics*, 1998, **110**, 95.
21 I. Abrahams, A. J. Bush, G. E. Hawkes and T. M. Nunes, *J. Solid State Chem.*, 1999, **147**, 631.
22 E. M. Levin and R. S. Roth, *J. Res. Nat. Bur. Stand. Sect. A*, 1964, **68**, 189.
23 C. N. R. Rao, G. V. Subba Rao and S. Ramdas, *J. Phys. Chem.*, 1969, **75**, 672.
24 H. A. Harwig and A. G. Gerards, *Thermochim. Acta*, 1979, **28**, 121.
25 T. Takahashi and H. Iwahara, *Mater. Res. Bull.*, 1978, **13**, 1447.
26 D. Risold, B. Hallstedt, L. J. Gauckler, H. L. Lukas and S. G. Fries, *J. Phase Equilib.*, 1995, **16**, 223.